Mathematics and Computers in Simulation 248 (2026) 291–301

Contents lists available at ScienceDirect

Mathematics and Computers in Simulation

journal homepage: www.elsevier.com/locate/matcom

Original articles

Parametric surface design for static solar concentration: Enhancing plastic waste pyrolysis in sustainable housing☆

E. Moreno [a], P. González-Rodelas [b,*], V. Pascual [c]

[a] CEMDATIC-E.T.S.I Telecommunication and Department of Structures and Building Physics, E.T.S.A. Polytechnic University of Madrid, Av. Juan de Herrera, Madrid, 28040, Spain
[b] Department of Applied Mathematics, University of Granada, Campus de Fuentenueva s/n, Granada, 18071, Spain
[c] Architectural Acoustics and Department of Structures and Building Physics, E.T.S.A. Polytechnic University of Madrid, Av. Juan de Herrera, Madrid, 28040, Spain

ARTICLE INFO

Keywords:
Mathematical framework
Parametric surface design
Static solar concentrators
Plastic pyrolysis
Sustainable housing

ABSTRACT

This paper develops a mathematical framework for the design of static parabolic solar concentrators with purely parametric geometries, aimed at replacing mechanically tracked systems. The central problem is to translate the apparent solar motion into a continuous parabolic surface whose focal line evolves consistently with the Sun's trajectory. We formulate the astronomical parameters (solar declination, hour angle, azimuth-elevation) and show how each parabola, defined in its local plane, is rotated and assembled into a complete surface through parametric transformations. To ensure smoothness and predictable reflection properties, the resulting point cloud is interpolated using spline-based methods that guarantee C^2 continuity, enabling reliable computation of tangents and normals. Practical implementation is achieved through an embedded device that verifies point placement during construction, bridging theoretical design with reproducible fabrication. While the broader motivation of this study is to address plastic waste through solar pyrolysis, the focus here is on the mathematical formulation that underpins the geometry and interpolation techniques necessary for building resilient, low-cost, and efficient static concentrators.

1. Introduction

In 2009, Johan Rockström and collaborators introduced the concept of planetary boundaries as a framework to define the limits that should not be exceeded to ensure the long-term stability of the Earth system and, consequently, human survival [1]. These boundaries, also referred to as environmental indicators, delineate a safe operating space for humanity. At the time of their introduction, seven of the nine boundaries were quantified, and three had already been transgressed. By 2015, this number of exceeded boundaries had increased to five, and more recent assessments confirm further deterioration, particularly in the category of *novel entities* [2].

The boundary of novel entities encompasses synthetic substances introduced into ecosystems, including persistent organic pollutants, heavy metals, radioactive waste, genetically modified organisms, and most prominently, plastics. This boundary is considered one of the most critical, as it implies that no substance should be released into the environment without full understanding of its long-term effects. Plastics have become ubiquitous across all ecosystems, being detected even in human placentas [3], while

☆ This article is part of a Special issue entitled: 'MATCOM_MACMAS 2025' published in Mathematics and Computers in Simulation.

* Corresponding author.
E-mail addresses: em.moreno@upm.es (E. Moreno), prodelas@ugr.es (P. González-Rodelas), valero.pascual@upm.es (V. Pascual).

https://doi.org/10.1016/j.matcom.2026.04.024
Received 23 November 2025; Received in revised form 19 April 2026; Accepted 20 April 2026
Available online 22 April 2026
0378-4754/© 2026 The Authors. Published by Elsevier B.V. on behalf of International Association for Mathematics and Computers in Simulation (IMACS). This is an open access article under the CC BY-NC-ND license (http://creativecommons.org/licenses/by-nc-nd/4.0/).

their toxicological effects impact multiple physiological systems [4]. Moreover, microplastics and nanoplastics are now pervasive in terrestrial, marine, and atmospheric environments, making exposure virtually unavoidable [5].

At the societal level, current waste management systems – particularly those dealing with plastic waste – have proven insufficient. This failure is reflected not only in environmental degradation but also in legal and political responses. Lawsuits against major corporations for misleading recycling claims [6], as well as public actions against waste management systems [7], illustrate the growing recognition of this issue. On a global scale, the cessation of plastic waste imports by China in 2021 has further worsened the accumulation of waste in industrialized countries [8]. In marine environments, the situation is particularly alarming: plastic particles have been found to outnumber zooplankton in certain regions, fundamentally altering ecological balances [9].

This crisis reflects a deeper structural contradiction between the paradigm of indefinite economic growth and the finite biophysical limits of the planet. As long as increasing production and disposable consumption are considered inherently positive, the plastic problem will persist. Although science and technology have historically provided solutions to complex challenges, there is no guarantee that they can sustain unlimited growth on a finite planet [10,11]. This stress is consistent with fundamental principles in physics, such as the Second Law of Thermodynamics and the limits imposed by the Uncertainty Principle, both of which highlight the existence of intrinsic constraints. Analogously, Earth's ecosystems impose non-negotiable limits on human activity [2,12].

Consequently, the plastic crisis cannot be addressed as a purely technological problem. Structural social and political transformations are required, including reductions in plastic production, policy changes, and cultural shifts away from disposable consumption patterns. In this context, the *doughnut economy* framework proposed by Raworth [13] offers a useful perspective, defining a safe and just operating space that balances human well-being with ecological constraints.

From a waste-management perspective, conventional mechanical recycling is not always a viable solution for plastic waste streams. It requires relatively clean and well-sorted materials and often leads to degradation of material properties after repeated cycles. In contrast, thermochemical processes such as pyrolysis can process heterogeneous and contaminated plastics, converting them into valuable products such as fuels, gases, and carbonaceous materials, while reducing the environmental impact associated with landfilling and incineration [14,15]. These characteristics make pyrolysis a promising pathway for the valorization of plastic waste.

Within this broader context, the present work focuses on a technological contribution based on solar-driven pyrolysis. Solar pyrolysis enables the degradation of thermoplastics into pyrolytic oils, gases, and carbon black, thereby reducing plastic waste while generating valuable products. Carbon black can be incorporated into cement-based materials to produce conductive composites [16], while pyrolytic oils can be refined into fuels [17]. Pyrolytic gases can also be used as alternative fuels in high-temperature industrial processes, reducing reliance on fossil energy sources.

However, conventional pyrolysis processes are typically driven by fossil-based or electrical heating, which limits their overall sustainability and increases their energy demand. In this context, the use of concentrated solar energy as a heat source has emerged as a promising alternative, enabling the direct conversion of solar radiation into high-temperature thermal energy while reducing carbon emissions and dependence on external fuels. Recent studies have demonstrated the feasibility and advantages of solar-driven pyrolysis systems, including improved thermal performance and energy efficiency through optimized reactor designs [18,19].

Despite these advances, the practical deployment of solar-driven pyrolysis systems remains strongly dependent on the design of efficient and robust solar concentration technologies. Most existing approaches rely on mechanically tracked systems to maintain alignment with the Sun, increasing system complexity, cost, and maintenance requirements. This limitation motivates the exploration of alternative solutions based on static geometries capable of capturing and concentrating solar radiation without moving parts. In this framework, the development of parametric static solar concentrators becomes a key enabling step toward scalable and low-maintenance solar pyrolysis systems.

From a practical perspective, static concentrators offer significant advantages: they eliminate mechanical failure modes, require minimal maintenance, and are more cost-effective to manufacture. Also, their robustness allows deployment in harsh environments characterized by strong winds, high salinity, or extreme climatic conditions, where active systems often fail.

From a mathematical standpoint, the design requires the precise formulation of astronomical parameters, including solar elevation, declination, hour, azimuth and zenith angles. These parameters define the solar trajectory at a given latitude and time of year. The mirror surface is constructed by defining a family of parabolas whose focal line evolves consistently with this trajectory. Each parabola is defined in a local plane and then transformed through rotations and translations governed by solar coordinates, generating a point cloud representation of the surface.

A key challenge in this construction is interpolation. While inverse-distance weighting [20] provides a simple reconstruction method, it lacks higher-order continuity and may lead to irregular curvature. To ensure predictable optical behavior, interpolation techniques with C^2 continuity, such as cubic and smoothing splines, are employed; enabling reliable computation of surface normals and stable reflection properties.

Finally, the transition from mathematical design to physical implementation is achieved through integration with embedded systems. The interpolation framework is coupled to an electronic device that guides the placement of points during mirror construction, ensuring that the theoretical design can be accurately reproduced in practice using open-source hardware.

The remainder of this paper is organized as follows. Section 2 introduces the mathematical modeling framework for the static parabolic mirror, detailing the astronomical parameters that determine its geometry and the transformations required to align the surface with the solar trajectory. Section 3 describes the distributed pyrolysis reactor and its integration with the mirror's focal line. Section 4 presents the validation methodology for the proposed model. Section 5 develops the interpolation framework, comparing inverse-distance approaches with the proposed spline-based methods and introducing the `ParabolaInterp` Arduino library. Finally, Section 6 summarizes the main contributions of this work and outlines potential directions for future research and practical deployment.

2. Mathematical model for the mirror

To design a mirror capable of focusing sunlight statically on the trajectory of plastics during a pyrolysis process, it is essential to understand the mechanisms that determine the position of the Sun. From this understanding, the concept of a parabolic mirror is employed to generate dynamic focal points, whose positions shift throughout the day in response to the apparent motion of the Sun. As a consequence, to ensure that the material undergoing pyrolysis receives the necessary thermal energy, it must be moved synchronously with the changing focal positions.

This leads to the concept of a distributed reactor, defined here as a spatially extended reactor aligned with the focal trajectory of the mirror, along which the material is progressively transported. In this configuration, the material moves in synchronization with the advancing focal point, ensuring continuous and homogeneous exposure to the thermal energy required for the pyrolytic transformation process.

The central technical challenge addressed in this work is therefore the design of solar concentrators that avoid the mechanical complexity and vulnerability of traditional tracking systems. The objective is to construct a static parabolic concentrator whose surface is mathematically defined to adapt to the solar trajectory without requiring moving parts, reducing the problem to the translation of solar motion into geometry.

To accurately design such a system, it is necessary to develop a parametric model of the parabolic mirror using mathematical functions. This model must account for the variations in the Sun's position throughout the day and over different seasons, including an accurate determination of solar elevation and azimuth angles using quadrant-consistent formulations. By deriving the functional relationships governing solar angles, true solar time, and focal point displacement, an optimized geometric configuration can be achieved. This approach ensures that the mirror efficiently directs sunlight onto the distributed reactor, maximizing energy transfer and enhancing the effectiveness of the pyrolysis process. Fig. 1 helps us understand the movement of the Sun over two different days of the year, one in winter and the other in summer. For energy density reasons, pyrolysis processes will always take place during the summer season, as the Sun's angle of incidence on the planet is more perpendicular. Additionally, the longer daylight hours allow for extended processing times, enabling the transformation of a greater amount of material. Let us start by defining some astronomical coordinates. The latitude of the location is a fundamental parameter, as it defines the position of the observer relative to the Earth's equatorial plane. Given a latitude ϕ, the solar angles are determined accordingly. In this study, we use a reference latitude of 37° (as an example), expressed in radians $\phi = \frac{37\pi}{180}$. To analyze the solar trajectory throughout the year, we define a transformation that converts the day number d_n (ranging from 1 to 365) into an angular measure $\beta\left[d_n\right]$, which accounts for the Earth's annual orbit around the Sun:

$$\begin{aligned}\beta &: \mathbb{N} \to \mathbb{R}\\ &d_n \mapsto \beta\left[d_n\right]\end{aligned}$$

where

$$\beta\left[d_n\right] = \frac{(d_n - 1)360}{365} \times \frac{\pi}{180}. \tag{1}$$

This formulation allows the alignment of daily solar positions with a periodic angular scale, facilitating precise calculations of solar angles. We also need the solar declination $\delta\left[d_n\right]$, which is the angle between the Earth's equatorial plane and the line connecting the Earth's center to the Sun. It varies approximately between −23.44° and +23.44° due to the axial tilt of the Earth. Spencer's empirical formula provides a highly accurate estimation of this angle:

$$\begin{aligned}\delta &: \mathbb{N} \to \mathbb{R}\\ &d_n \mapsto \delta\left[d_n\right]\end{aligned}$$

where

$$\begin{aligned}\delta\left[d_n\right] = {} & 0.006918 - 0.399912\cos(\beta\left[d_n\right]) + 0.070257\sin(\beta\left[d_n\right]) - 0.006758\cos(2\beta\left[d_n\right])\\ & + 0.000907\sin(2\beta\left[d_n\right]) - 0.002697\cos(3\beta\left[d_n\right]) + 0.00148\sin(3\beta\left[d_n\right]).\end{aligned} \tag{2}$$

This expression incorporates multiple harmonic terms (sine and cosine functions) that adjust the annual periodicity of solar declination with high precision. The coefficients in the equation are derived from astronomical observations, ensuring accuracy in tracking seasonal variations. The determination of $\delta\left[d_n\right]$ is crucial for calculating the Sun's position relative to a fixed latitude, which is essential in the design of static parabolic mirrors adapted to the solar trajectory. By utilizing this model, it is possible to develop a geometric configuration that effectively concentrates solar radiation over an extended period without requiring mechanical adjustments. Another important parameter is the true solar time, which does not always coincide with the local time. The true solar time (TST) is directly related to the Sun's position relative to the local meridian and is expressed in terms of the hour angle. The hour angle represents the angular displacement of the Sun with respect to the local meridian, measured in degrees or radians. In this way, the hour angle $timeH$ in radians can be determined using the following equation:

$$\begin{aligned}timeH &: \mathbb{R} \to \mathbb{R}\\ &TST \mapsto H\left[TST\right]\end{aligned}$$

where

$$timeH\,[TST] = \left(\frac{15\pi}{180}\right)(TST - 12). \tag{3}$$

In the last equation:

- 15° represents the angular equivalent of one solar hour.
- TST is the true solar time in decimal format (e.g., 13.5 for 13:30).
- Subtracting 12 centers the system at solar noon, where the hour angle is zero.

This hour angle is essential for determining the Sun's position in the sky and plays a crucial role in the computation of both solar elevation and azimuth angles, which are fundamental for designing passive solar tracking systems such as parabolic mirrors. To transform the local solar time (LST) into true solar time (TST), we must account for:

1. The geographical longitude of the location ξ.
2. The central meridian longitude of the time zone ξ_{st}.
3. The equation of time (ET), which corrects discrepancies between mean and true solar time.

The conversion formula is:

$$TST : \mathbb{N} \times \mathbb{R}^3 \to \mathbb{R}$$
$$(d_n, LST, \xi_{st}, \xi) \mapsto TST\left[d_n, LST, \xi_{st}, \xi\right]$$

where

$$TST\left[d_n, LST, \xi_{st}, \xi\right] = LST + \frac{4(\xi_{st} - \xi) + ET[d_n]}{60} \tag{4}$$

with

$$ET : \mathbb{N} \to \mathbb{R}$$
$$d_n \mapsto ET\left[d_n\right]$$

where

$$ET\left[d_n\right] = 9.87\sin(2\beta\left[d_n\right]) - 7.53\cos(\beta\left[d_n\right]) - 1.5\sin(\beta\left[d_n\right]). \tag{5}$$

The transformation of local solar time into true solar time is fundamental for modeling the Sun's position in real hour-angle coordinates. This conversion is essential in:

- Determining the hour angle, which influences the design and orientation of solar systems.
- Optimizing the efficiency of static solar concentrators by accurately aligning them with the Sun's trajectory.

Also, the solar position at a given moment depends on multiple parameters, including the latitude θ, the hour of the day TST, and the day of the year d_n. These factors determine the solar elevation angle h and the azimuth angle ϕ, which describe the Sun's apparent position in the sky. The declination angle, represented by $\delta(d_n)$, varies throughout the year and modifies the solar trajectory accordingly. The solar elevation angle $h(d_n, TST)$ is defined as follows:

$$h : \mathbb{N} \times \mathbb{R} \to \mathbb{R}$$
$$(d_n, TST) \mapsto h[d_n, TST]$$

where

$$h[d_n, TST] = \arcsin\left[\sin(\theta)\sin(\delta(d_n)) + \cos(\theta)\cos(\delta(d_n))\cos(\text{timeH}(TST))\right]. \tag{6}$$

The solar zenith angle θ_z is defined as:

$$\theta_z : \mathbb{N} \times \mathbb{R} \to \mathbb{R}$$
$$(d_n, TST) \mapsto \theta_z[d_n, TST]$$

where

$$\theta_z[d_n, TST] = \arccos\left[\cos(\theta)\cos(\delta(d_n))\cos(\text{timeH}(TST)) + \sin(\theta)\sin(\delta(d_n))\right]. \tag{7}$$

The solar azimuth angle ϕ is computed using a quadrant-aware formulation based on the horizontal projection of the solar direction:

$$\phi(d_n, TST) = \text{atan2}\left(\cos(\delta(d_n))\sin(\text{timeH}(TST)),\ \cos(\theta)\sin(\delta(d_n))\right.$$
$$\left. - \sin(\theta)\cos(\delta(d_n))\cos(\text{timeH}(TST))\right). \tag{8}$$

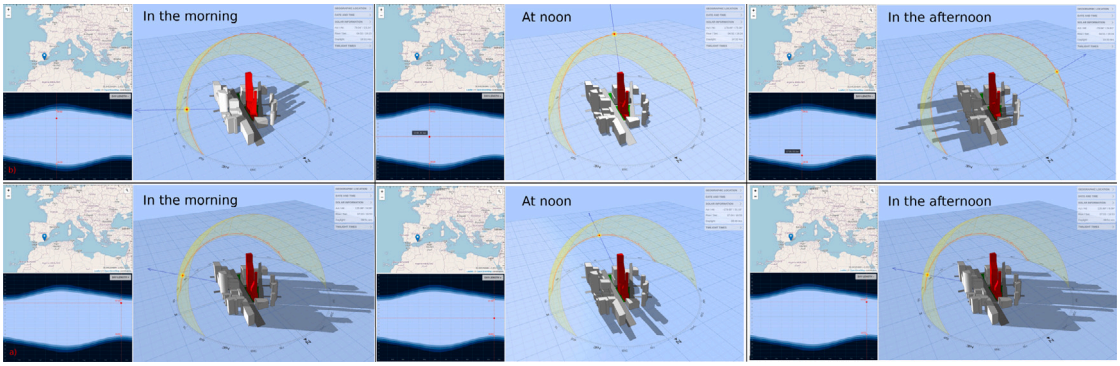


Fig. 1. The solar trajectory in terms of azimuth and elevation for a given latitude has been illustrated using the 3D Sun-Path tool from the andrewmarsh.com website. The background map is provided by Google Maps, allowing for a clear visualization of the Sun's movement throughout the day for a specific location. This representation helps to understand the importance of deriving the essential functional relationships for the Sun's position in terms of azimuth and altitude for a given latitude on a particular day of the year. Such relationships are crucial for determining the parametric surface of a mirror like the one described in this study.

This formulation ensures correct quadrant resolution and is consistent with standard solar position algorithms, such as the Solar Position Algorithm (SPA) developed by Reda and Andreas [21], as well as the widely used SOLPOS implementation provided by NREL [22,23].

However, for the geometric construction of the mirror surface, a signed planar angle consistent with the model reference frame is required. Therefore, a derived geometric azimuth $\phi_g(d_n, TST)$ is introduced. It is defined as the signed angle in the horizontal plane obtained from the projection of the solar direction onto the local xy-plane of the model. This angle is measured from the positive x-axis in a counterclockwise direction and varies continuously over the daily solar trajectory.

This geometric azimuth is derived from the physical solar azimuth ϕ and preserves the solar direction while providing a continuous angular parameter consistent with the reference frame adopted for the parametric generation of the mirror surface.

We have to consider that in Eqs. (7) and (8) the following definitions apply: θ is the latitude of the observer, $\delta(d_n)$ is the solar declination angle, which depends on the day of the year d_n, and $\text{timeH}(TST) = \frac{15\pi}{180}(TST - 12)$ is the hour angle, which depends on the true solar time TST.

The following equations generate a planar representation of the solar trajectory for a specific day and a given latitude. These equations allow us to understand how the position of the Sun varies throughout the day (in plan view), which is essential for the design of solar systems and parabolic mirrors. We begin by defining a coordinate system in which:

- $x[d_n, TST]$-coordinate represents the projection along the east–west axis.

$$x[d_n, TST] = \cos(h[d_n, TST])\cos(\phi_g[d_n, TST]) \tag{9}$$

- $y[d_n, TST]$-coordinate represents the projection along the north–south axis.

$$y[d_n, TST] = \cos(h[d_n, TST])\sin(\phi_g[d_n, TST]) \tag{10}$$

where $\phi_g[d_n, TST]$ denotes the geometric azimuth introduced previously, defined in the local coordinate system of the model.

To construct the parabolic mirror in the real world, we need a point cloud that serves as a basis for interpolation, allowing us to represent the mirror's coordinates in physical space. This will be achieved using a tool that will be described in a later section and in the Supplementary Material of this article. Therefore, what we will outline next are the coordinates of these points and the procedure used to obtain them. To accomplish this goal, the first step is to define an operator that, given a set of points, applies a rotation by a specified angle followed by a translation.

$$\begin{aligned}&\text{TrCurve} : \mathbb{R}^m \times \mathbb{R}^3 \to \mathbb{R}^m\\ &(\text{points}, \alpha, \Delta_x, \Delta_y) \mapsto \text{NewPoints} \equiv \text{TrCurve}[\text{points}, \alpha, \Delta_x, \Delta_y]\end{aligned}$$

where

$$\text{TrCurve}[\text{points}, \alpha, \Delta_x, \Delta_y] = \begin{pmatrix}\cos(\alpha)x_i - \sin(\alpha)y_i + \Delta_x\\ \sin(\alpha)x_i + \cos(\alpha)y_i + \Delta_y\\ z_i\end{pmatrix}^{\top} \qquad \forall i = 1, \dots, m. \tag{11}$$

The set of points consists of m elements and is given by:

$$\text{points} \equiv \{(x_1, y_1, z_1), \dots, (x_i, y_i, z_i), \dots, (x_m, y_m, z_m)\}. \tag{12}$$

The transformed points NewPoints represent the same initial set of points after a rotation and translation. The rotation is applied by an angle α to ensure that the incident solar rays are locally perpendicular to the parabolic mirror surface. The translation parameters Δ_x and Δ_y displace the parabolas so that they are correctly positioned along the solar trajectory in the horizontal plane. To achieve this goal of rotating each fabricated parabola by an angle such that it remains perpendicular to the Sun at each considered point on the surface, the required rotation angle must correspond to the geometric azimuth of the Sun at that particular hour, but with opposite sign:

$$\alpha = -\phi_g[d_n, TST].$$

This ensures consistency with the local coordinate system used to define the planar solar trajectory. This adjustment is necessary because the reflection process imposes a symmetry between the incident and reflected rays, requiring the mirror orientation to compensate the solar azimuthal variation, meaning that when the azimuth rotates by a given angle, the parabolic profile must rotate by the same angle but in the opposite direction. Consequently, assuming a left-handed (levorotatory or counterclockwise) solar trajectory in plan view during sunrise, the parabola's rotation must follow a right-handed (dextrorotatory or clockwise) movement throughout the day to maintain perpendicular alignment with incoming sunlight.

Also, the displacements Δ_x and Δ_y for each point at a given true solar time (TST) correspond to the planar coordinates of the Sun's position at that specific moment. Mathematically, these displacements are defined as:

$$\Delta_x = x[d_n, TST],$$
$$\Delta_y = y[d_n, TST].$$

This ensures that each parabolic mirror is aligned along the Sun's projected path in the horizontal plane, allowing for an optimized solar concentration system. The construction of each parabolic profile will be carried out in the XZ plane at the coordinate $y = 0$, following a parametric procedure in which the parameter t will be swept. If we have a set of $L \in \mathbb{N}$ values of the parameter t, we will then obtain a set of L pairs $x_{\text{points-profile}}[d_n, TST, t]$ and $z_{\text{points-profile}}[d_n, TST, t]$, which will allow us to define the coordinates in the XZ plane of the parabola necessary to focus sunlight at a specific time on a particular day of the year at a given latitude. The functional forms are as follows:

$$\begin{aligned}\left(x_{\text{points-profile}}, y_{\text{points-profile}}\right) &: \mathbb{N} \times \mathbb{R}^2 \to \mathbb{R}^2 \\ (d_n, TST, t) &\mapsto \left(x_{\text{points-profile}}[d_n, TST, t], y_{\text{points-profile}}[d_n, TST, t]\right)\end{aligned}$$

where

$$\begin{aligned}&\left(x_{\text{points-profile}}[d_n, TST, t], y_{\text{points-profile}}[d_n, TST, t]\right) = \\ &\begin{pmatrix} t\cos(\theta_z[d_n, TST]) - \frac{t^2}{4f}\sin(\theta_z[d_n, TST]) \\ t\sin(\theta_z[d_n, TST]) + \frac{t^2}{4f}\cos(\theta_z[d_n, TST]) \end{pmatrix}^{\top}, \qquad \forall t \in \mathbb{R}.\end{aligned} \tag{13}$$

The coordinates of the focal point are defined in the local coordinate system of the parabola, i.e., relative to its vertex in the XZ profile plane before any global rotation or translation is applied.

$$\begin{aligned}\left(f_x, f_y\right) &: \mathbb{N} \times \mathbb{R} \to \mathbb{R}^2 \\ (d_n, TST) &\mapsto \left(f_x[d_n, TST], f_y[d_n, TST]\right)\end{aligned}$$

where

$$\left(f_x[d_n, TST], f_y[d_n, TST]\right) = \begin{pmatrix} -f\cos(h[d_n, TST]) \\ f\sin(h[d_n, TST]) \end{pmatrix}^{\top}. \tag{14}$$

Here, f represents the focal distance of the parabolic mirror.

The focal trajectory, also defined by a set of points, corresponds to the coordinates necessary for the arrangement and positioning of the distributed reactor, which is described in the following section.

3. Distributed pyrolysis reactor and parametric mirror focus

To fully understand the operational procedure of this mirror, we refer to Fig. 2, which illustrates how focal points are generated as the Sun progresses in its daily motion. In the morning, we can observe that the focal point forms at the easternmost position. However, it is important to note that this is not the only point that forms at sunrise; rather, there is a continuous linear distribution of focal points that does not necessarily coincide with the discrete focal points depicted in Fig. 2. The points shown in the figure correspond to specific configurations at each true solar time (hours). Throughout the day, the actual focal line that forms at each instant closely follows the trajectory drawn in Fig. 2. While there may be slight deviations, this is not particularly significant because the mass of plastics undergoing pyrolysis will move along the focal trajectory. By positioning the reactor at the exact location where convergence occurs, we ensure that solar intensity is maximized, optimizing energy absorption within the distributed reactor.

The concept of a distributed reactor is better understood through Fig. 3, which highlights that this is not a static reactor but rather a dynamic one. Instead of relocating the entire system (reactor) to the heat source, the process operates by moving the plastic

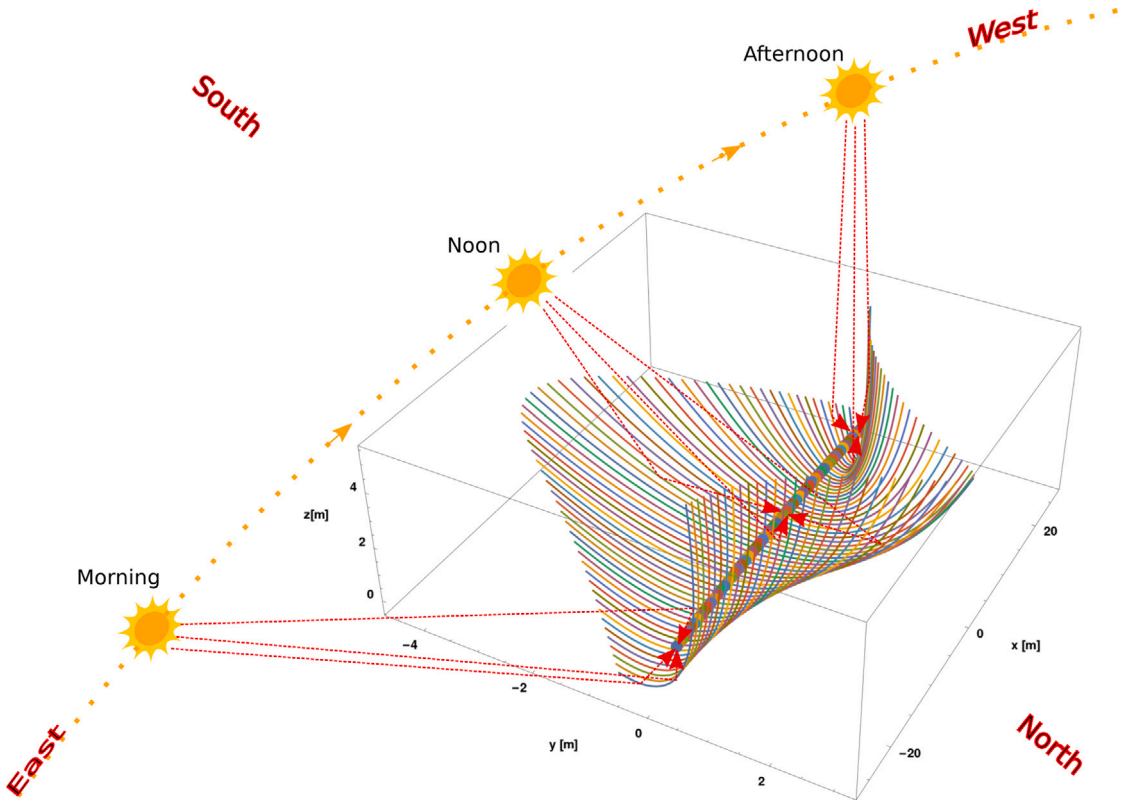


Fig. 2. The figure illustrates how, along the Sun's east-to-west trajectory, multiple geometric lines trace the path followed by a beam of sunlight at different times of the day—morning, noon, and afternoon. These lines correspond to the optical-geometric configuration that focuses sunlight at each true solar time onto the focal point of the parabola (a particular one). This focal point aligns with the position of the pyrolytic plastic within the distributed reactor, ensuring optimal energy concentration for the pyrolysis process.

mass itself to the focal points where sufficient energy is available for the pyrolysis reaction. This is achieved through an auger screw, as illustrated in Fig. 3, driven by a motor synchronized with the focal point positions throughout the day based on true solar time.

This distributed reactor can be considered a practical solution to a significant challenge: maintaining a high and stable temperature in the region where pyrolysis occurs. Traditionally, this has been achieved using complex solar tracking systems, which are highly sensitive to meteorological conditions, particularly wind. Despite their robust design and manufacturing, these systems require constant maintenance and repairs. In contrast, the proposed static system, though exposed to the elements, remains inherently stable since all moving components are contained within the system itself. As a result, it offers significantly greater durability and resilience against adverse weather conditions while also reducing long-term costs. This cost reduction is not only due to lower maintenance requirements but also to the fundamental simplicity of the operational system compared to a dynamic solar tracking system. The key advantage of employing a fully static solar tracking system, where movement occurs within the reactor – or specifically within the section containing the pyrolytic material undergoing transformation – is that heat is concentrated precisely where it is needed. Additionally, considering that meteorological intermittency is a major challenge in solar pyrolysis, this technology ensures that operational feasibility is not restricted to specific days with ideal weather conditions. Despite being a completely passive and immobile mirror, its ability to focus sunlight on the distributed reactor extends well beyond a single day. The system operates over an extended summer interval, spanning from late May to mid July, during which day-to-day variations in the solar trajectory remain sufficiently small. This allows a single static mirror geometry to maintain effective focusing performance throughout the entire period. Rather than relying on short, discrete operational windows, the design ensures continuous functionality over several consecutive weeks centered around the summer solstice. This extended stability is a key feature of the proposed approach, enabling practical deployment without the need for mechanical adjustment or reconfiguration.

Until now, we have assumed that the existence of such mirrors is entirely feasible. However, the practical execution of a surface like this presents a significant challenge, especially when attempting to construct it using a puzzle-like approach. This means, for example, employing masonry, where numerous small elements must be precisely positioned to form a complex surface. While this surface exhibits certain symmetries, its construction is far from straightforward, as there are no intuitive reference points for making accurate measurements that guide the placement of these masonry elements. Furthermore, once the structure is built, it must be coated and finished to support a reflective material or mirror-like fabric. This necessity adds another layer of complexity, requiring a methodology that is both cost-effective and practical for the real-world construction of such surfaces. In the Supplementary Material

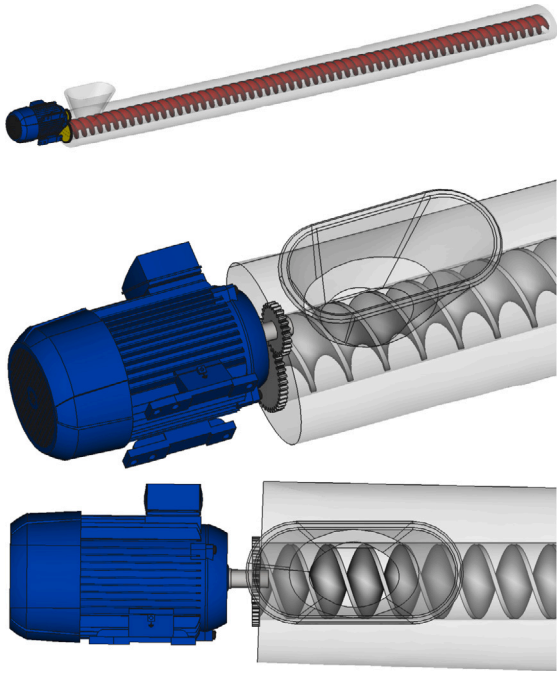


Fig. 3. From the upper to the lower part of the figure, the distributed reactor is shown. Along the trajectory followed by the focal point—where solar energy is concentrated each hour by the corresponding parabola at that True Solar Time (TST)—a curve has been used as a guide to extrude an ellipse, forming the body of the reactor. This design allows for the integration of a perfectly rectilinear cylindrical element, the auger screw, within the curved structure, specifically within the extruded ellipsoid. The figure also shows the hopper, through which the auger screw is loaded with plastic materials. Additionally, as depicted, an electric motor with a coplanar gear system amplifies the motor's force through its configuration, enabling the controlled movement of the pyrolytic mass along the pyrolysis process. This ensures that the material is precisely positioned at the location where the main heat source, determined by true solar time, is concentrated.

accompanying this article we also introduce a device that makes this process feasible by utilizing the same points that define the surface itself.

4. Model validation

The validation of the proposed optical–thermal model is carried out in three sequential steps: (i) geometric validation through ray tracing, (ii) verification of energy interception within the reactor region, (iii) computation of the spatial power-density distribution on the reactor surface and (iv) temperature calculation.

The complete formulation of the geometric and energy interception model, including the ray-tracing procedure and numerical implementation, is provided in the Supplementary Material and in the GitHub repository associated with this work [24].

5. Interpolation

In order to practically implement the parametric geometry of the parabolic mirror on a rooftop installation, it is necessary to translate the theoretical curve into a discrete set of reference points. This process requires the use of interpolation techniques, with spline-based methods being particularly well-suited for ensuring both accuracy and smoothness of the reconstructed surface [25–29]. The interpolation is directly linked to the electronic device described in the Supplementary Material, as the Arduino platform is responsible for positioning and verifying each construction element in real space. To facilitate reproducibility and transparency, all mathematical functions developed for spline interpolation, together with the complete Arduino programming framework and auxiliary files, are available in an open-access repository [24]. This repository contains both the Wolfram Mathematica notebook and the embedded code, thereby providing the necessary resources for extending, adapting, or replicating the proposed methodology in future implementations.

5.1. Spline-based interpolation for on-site parabolic profiling

Preprocessing and local profile extraction. Let $\{(x_i, y_i, z_i)\}_{i=1}^{N}$ be the point cloud stored on the SD card and measured/used on site. We first remove the device tilt using the appropriate pitch and roll angles in the Inertial Measurement Unit (IMU) by applying a rigid

rotation $R_{\mathrm{IMU}} \in SO(3)$ so that the ground plane becomes $z = 0$. Denote corrected points $(\bar{x}_i, \bar{y}_i, \bar{z}_i) = R_{\mathrm{IMU}}(x_i, y_i, z_i)$. For a target azimuth $\theta^\star$ (set by the azimuth servo) we rotate about the vertical axis by $R_z(-\theta^\star)$ to define a local profile plane $\Pi(\theta^\star)$ where the parabola is observed head-on. Let $(x'_i, y'_i, z'_i) = R_z(-\theta^\star)(\bar{x}_i, \bar{y}_i, \bar{z}_i)$. We select a thin profile strip by $|y'_i| \le \varepsilon_\theta$ and project onto the profile plane by $u_i := x'_i,\ w_i := z'_i$. As the mirror cross-section is designed to be parabolic with a single concavity, the data $\{(u_i, w_i)\}$ forms a (noisy) sample of a graph $w = f(u)$ on an interval $[u_{\min}, u_{\max}]$.

Spline model. We fit a cubic smoothing spline $S(u)$ to the samples $\{(u_i, w_i)\}_{i=1}^{M}$ ($M \le N$ in the strip) by solving

$$S \;=\; \arg\min_{g \in \mathcal{H}^2} \sum_{i=1}^{M} \big(w_i - g(u_i)\big)^2 \;+\; \lambda \int_{u_{\min}}^{u_{\max}} \big(g''(u)\big)^2\, du,$$

where $\lambda \ge 0$ tunes noise rejection vs. fidelity. In the low-noise regime we set $\lambda = 0$ and use the natural cubic interpolant with $S''(u_{\min}) = S''(u_{\max}) = 0$; in presence of measurement noise we pick $\lambda > 0$ to obtain a C^2 curve with controlled curvature. The fitted spline provides S, S', S'' everywhere on $[u_{\min}, u_{\max}]$, ensuring smooth normals and predictable convexity.

Parabolic priors (optional constraint). If a design focal distance f is specified for the profile, we can weakly regularize toward a parabola opening upward:

$$\min_{S} \sum_{i=1}^{M} \big(w_i - S(u_i)\big)^2 + \lambda \int (S''(u))^2 du \;+\; \mu \int \big(S(u) - \tfrac{(u-u_0)^2}{4f} - w_0\big)^2 du,$$

with small $\mu > 0$ and axis (u_0, w_0) given by layout, preserving data-driven fit while stabilizing the opening.

Ray–curve intersection as range prediction. In the local profile plane $\Pi(\theta^\star)$ the LiDAR ray for polar elevation $\phi^\star$ (servo) is

$$\ell(s) = s\, d', \qquad d' = (\cos\phi^\star,\ \sin\phi^\star), \quad s \ge 0,$$

expressed in (u, w)-coordinates. The mirror profile is the spline curve $\gamma(u) = (u, S(u))$. We estimate the range $s^\star$ by orthogonal projection of ℓ onto γ:

$$u^\star \;=\; \arg\min_{u \in [u_{\min}, u_{\max}]} \operatorname{dist}^2\big(\gamma(u),\, \ell\big) \;=\; \arg\min_{u}\Big(\|\gamma(u)\|^2 - \big(\gamma(u)\cdot d'\big)^2 \Big),$$

and then

$$s^\star \;=\; \gamma(u^\star)\cdot d' \;=\; u^\star \cos\phi^\star + S(u^\star)\sin\phi^\star.$$

We compute $u^\star$ via a safeguarded Newton method using S', S'':

$$F(u) := \nabla_u\Big(\|\gamma(u)\|^2 - (\gamma(u)\cdot d')^2 \Big) \;=\; 2\,\gamma'(u)\cdot\Big(\gamma(u) - (\gamma(u)\cdot d')\, d'\Big),$$

$$u_{k+1} \;=\; \Pi_{[u_{\min}, u_{\max}]}\big(u_k - \eta\, F(u_k)/F'(u_k)\big),$$

with step size $\eta \in (0, 1]$ and interval projection Π; $F'(u)$ is obtained by differentiating F using S', S'' (details and references in appendix of the Supplementary Material). Convergence is accelerated by initializing u_0 as the closest sample abscissa to the current ray, and capping iterations.

Acceptance and feedback. Given the measured range $\hat{s}$ and predicted $s^\star$, we define the placement error

$$e := \hat{s} - s^\star.$$

The controller in the electronic device triggers haptic/aural feedback when $|e| \le \tau$ (tolerance), and displays $\phi^\star, \theta^\star, u^\star, S(u^\star)$ on the LCD for operator guidance. The ground-plane constraint ($w \ge 0$) is enforced by rejecting any u such that $S(u) < 0$ and by clipping the ray to $s \ge 0$.

5.2. Implementation and availability

Two alternative Arduino codes are provided to illustrate the interpolation step on site. The first corresponds to the original implementation, where the interpolation of the local point cloud was carried out using an inverse-distance weighted average of the eight nearest neighbors (referred to as the *ESPESO* method, see [20] for an adaptive version). The second corresponds to the updated implementation described above, where the interpolation is spline-based, enforcing C^2 smoothness and parabolic convexity.

To facilitate maintenance and reduce code duplication, we have also developed an independent Arduino library, named `ParabolaInterp`, which encapsulates both strategies (ESPESO and spline) under a common interface. By setting a single configuration flag, the user can switch between the two interpolation modes at compile time. Both Arduino codes ("`Code_ESPESO.ino`" and "`Code_Spline.ino`") as well as the `ParabolaInterp` library are openly accessible in the companion repository [24].

6. Conclusions

The three main contributions of this work are as follows:

1. Parametric Curve Design for Static Solar Concentration: A parametric curve is developed that allows a static mirror to concentrate sunlight for an entire week, following the Sun's trajectory without requiring movement. This results in an efficient system tailored for distributed pyrolysis reactors.
2. Practical Construction Methodology: A practical framework is proposed for the construction of these mirrors, accounting for necessary error margins to ensure feasibility and effectiveness in real-world implementation.
3. Urban Integration of Pyrolysis: The most significant contribution is the conceptualization of solar pyrolysis in an urban environment. A sequential usage strategy for the reactors is introduced to prevent toxic emissions and urban heat islands, necessitating site-specific geometric designs for each rooftop based on two distinct operational time windows throughout the year. Additionally, the study proposes storing plastic waste on building rooftops, repurposing it as insulating material, thereby integrating functionality and sustainability into the overall solution.

CRediT authorship contribution statement

E. Moreno: Writing – original draft, Methodology, Conceptualization. **P. González-Rodelas:** Writing – review & editing, Validation, Investigation, Formal analysis. **V. Pascual:** Visualization, Software, Data curation.

Acknowledgments

The first author would like to express his gratitude to Natalia Martínez, whose undergraduate thesis work provided the inspiration and conceptual foundations for the development of this work. Second author also acknowledges the financial support from the University of Granada, Spain (through the "Plan Propio de Investigación *y* Transferencia") and the Andalusian Research Group FQM-191.

Appendix A. Supplementary data

Supplementary material related to this article can be found online at https://doi.org/10.1016/j.matcom.2026.04.024.

References

[1] Johan Rockström, Will Steffen, Kevin Noone, Åsa Persson, F. Stuart Chapin, Eric F. Lambin, Timothy M. Lenton, Marten Scheffer, Carl Folke, Hans Joachim Schellnhuber, Björn Nykvist, Cynthia A. de Wit, Terry Hughes, Sander van der Leeuw, Henning Rodhe, Sörlin Sverker, Peter K. Snyder, Robert Costanza, Uno Svedin, Malin Falkenmark, Louise Karlberg, Robert W. Corell, Victoria J. Fabry, James Hansen, Brian Walker, Diana Liverman, Katherine Richardson, Paul Crutzen, Jonathan A. Foley, A safe operating space for humanity, Nature 461 (7263) (2009) 472–475.
[2] Antonio Turiel, El futuro de Europa, Destino, 2024.
[3] Marcus A. Garcia, Rui Liu, Alex Nihart, Eliane El Hayek, Eliseo Castillo, Enrico R. Barrozo, Melissa A. Suter, Barry Bleske, Justin Scott, Kyle Forsythe, Jorge Gonzalez-Estrella, Kjersti M. Aagaard, Matthew J. Campen, Quantitation and identification of microplastics accumulation in human placental specimens using pyrolysis gas chromatography mass spectrometry, Toxicol. Sci. 199 (1) (2024) 81–88.
[4] Bosen Zhao, Palizhati Rehati, Zhu Yang, Zongwei Cai, Caixia Guo, Yanbo Li, The potential toxicity of microplastics on human health, Sci. Total Environ. 912 (2024) 168946.
[5] Laura Parker, The world's plastic pollution crisis, explained, 2023, nationalgeographic.com.
[6] Rob Bonta, Attorney general bonta sues exxonmobil for deceiving the public on recyclability of plastic products, State Calif. Dep. Justice (2024).
[7] Julio Barea Luchena, Estas 5 mentiras de ecoembes te van a sorprender, 2010, es.greenpeace.org/.
[8] Kenneth Rapoza, China doesn't want the world's trash anymore. Including 'recyclable' goods, Forbes (2021).
[9] C. Moore, Plastic Ocean: How a Sea Captain's Chance Discovery Launched a Determined Quest To Save the Oceans, Penguin Publishing Group, 2011.
[10] D.H. Meadows, Club of Rome, The Limits to Growth: A Report for the Club of Rome's Project on the Predicament of Mankind, A Potomac Associates book. Universe Books, 1974.
[11] D.H. Meadows, J. Randers, D.L. Meadows, the Limits To Growth: The 30-Year Update, Chelsea Green Publishing Company, 2004.
[12] Ignacio de Blas, Margarita Mediavilla, Iñigo Capellán-Pérez, Carmen Duce, The limits of transport decarbonization under the current growth paradigm, Energy Strat. Rev. 32 (2020) 100543.
[13] K. Raworth, Doughnut Economics: Seven Ways to Think Like a 21st-century Economist, Random House Business Books, 2017.
[14] Ruming Pan, Jie Yu, Youwei Yang, Ilman Nuran Zaini, Xibo He, Muhammad Rafique, Yibo Wu, Kuandong Jiang, Leilei Dai, Yi Fang, Youchuang Chao, Yuming Wen, Yanming Guo, Gérald Debenest, Weihong Yang, Wangliang Li, Yaning Zhang, Yong Shuai, Enhancing carbon nanotubes production from pyrolysis-catalysis of plastic waste through monolithic heating, Natl. Sci. Rev. (2026) Advance article/original unedited manuscript.
[15] Youwei Yang, Ruming Pan, Yibo Wu, Qinghui Pan, Yong Shuai, A porous media catalyst for waste polyethylene pyrolysis in a continuous feeding reactor, Energy 302 (2024) 131855.
[16] Nicolas Chanut, Damian Stefaniuk, C. Weaver James, Yunguang Zhu, Yang Shao-Horn, Admir Masic, Franz-Josef Ulm, Carbon–cement supercapacitors as a scalable bulk energy storage solution, Proc. Natl. Acad. Sci. 120 (32) (2023) e2304318120.
[17] Kris De Decker, Plastic waste in the fuel tank?, Low Tech Magazine (2023).
[18] Ruming Pan, Youwei Yang, Bachirou Guene Lougou, Lianxuan Wu, Wei Wang, Yanming Guo, Yong Shuai, Thermal performance evaluation of a novel solar-driven pyrolysis reactor, Energy 313 (2024) 134051.
[19] Youwei Yang, Ruming Pan, Yuhan Jin, Yibo Wu, Qinghui Pan, Yanming Guo, Yong Shuai, Modelling of a surface-absorption fixed-bed solar-driven reactor for waste plastics pyrolysis, Appl. Therm. Eng. 292 (2026) 130444.
[20] George Y. Lu, David W. Wong, An adaptive inverse-distance weighting spatial interpolation technique, Comput. Geosci. 34 (9) (2008) 1044–1055.
[21] Ibrahim Reda, Afshin Andreas, Solar position algorithm for solar radiation applications, Sol. Energy 76 (5) (2004) 577–589.

[22] John A. Duffie, William A. Beckman, Solar Engineering of Thermal Processes, Wiley, 2013.
[23] William Martin, et al., Solpos 2.0: Solar Position and Intensity Code, Technical Report NREL/TP-560-34302, National Renewable Energy Laboratory (NREL, 2001.
[24] E. Moreno, P. González-Rodelas, V. Pascual, Repository: Mathematica Notebook and Arduino Code, 2025, http://dx.doi.org/10.5281/zenodo.19440007.
[25] Carl de Boor, A Practical Guide to Splines, in: Applied Mathematical Sciences, vol. 27, Springer, revised edition, 2001.
[26] M.A. Fortes, P. González, A. Palomares, M. Pasadas, Filling holes with geometric and volumetric constraints, Comput. Math. Appl. 74 (4) (2017) 671–683.
[27] M.A. Fortes, P. González, A. Palomares, M.L. Rodríguez, Filling holes using a mesh of filled curves, Math. Comput. Simulation 164 (2019) 78–93.
[28] Pedro González, Hasan Idais, Miguel Pasadas, Mohammed Yasin, Evolutionary computation for optimal knots allocation in smoothing splines of one or two variables, Int. J. Comput. Intell. Syst. 11 (1) (2018) 1294–1306.
[29] Larry L. Schumaker, Spline Functions: Basic Theory, third ed., Cambridge University Press, 2007.